Journal of Hazardous Materials, 18 (1988) 37–67
Elsevier Science Publishers B.V., Amsterdam — Printed in The Netherlands

FLUID MODELING OF DENSE GAS DISPERSION OVER A RAMP

REX E. BRITTER

Department of Engineering, University of Cambridge, Cambridge CB2 1PZ (Great Britain)

and WILLIAM H. SNYDER*

Meteorology and Assessment Division, Atmospheric Sciences Research Laboratory, U.S. Environmental Protection Agency, Research Triangle Park, NC 27711 (U.S.A.)

(Received April 15, 1987; accepted August 1987)

Summary

The basic nature of the transport and dispersion of a dense gas plume in the simulated neutral atmospheric boundary layer of a wind tunnel was investigated, both in flat terrain and over a ramp. Measurements were made of the concentration fields downstream of a ground-level, circular source; these measurements consisted of longitudinal ground-level, vertical, and crosswind profiles at various distances downwind. Both neutrally buoyant (air) and negatively buoyant (CO_2) source gases were used so that the specific effects of the density difference could be observed. Similarly, measurements were made in both flat terrain and over the ramp (14° slope followed by an elevated plateau) so that specific effects of the terrain could be observed. Flow visualization was done to ascertain that the dense plume was turbulent, hence, that the effects of molecular properties were insignificant. For the particular value of the buoyancy parameter used in these experiments, the plume buoyancy was significant; the resulting dense plume was significantly wider in the lateral direction and much narrower in the vertical direction, yet the longitudinal ground-level concentration profile downwind was essentially identical to that from the neutral plume. The lateral concentration profiles of the neutral plumes were essentially Gaussian in character, whereas the dense gas plumes exhibited top-hat distributions for considerable distances from the source. The vertical concentration profiles of the neutral plumes were not Gaussian, but displayed variations of the form $C/C_{mx}=\exp(-Az^n)$ with $n\simeq 1.5$. On the other hand, the dense gas plumes displayed vertical variations of the form $C/C_{mx}=\exp[-z/\bar{z}]$, where $\bar{z}$ is the centroid of the distribution. The net effect of the ramp on the dense gas plume was a small reduction in ground-level concentration (less than a factor of two, even for a source relatively close to the base of the ramp). This reduction was quite similar to that observed for the neutral plume.

1. Introduction

Toxic and hazardous materials, when accidentally released, frequently lead to clouds or plumes that have a density different from the environment. When

*On assignment from the National Oceanic and Atmospheric Administration, U.S. Department of Commerce.

0304-3894/88/$03.50

the release has a smaller density than the environment (positively buoyant), the gas will rise away from the ground and populated areas, generally producing low ground-level concentrations. The release of material that is neutrally buoyant (the same density as the environment) has been extensively studied (e.g., Ref. [1,2]), although the release conditions (large volume, time-dependent) often preclude the simple application of these results. Negatively buoyant releases can produce clouds or plumes that cover large surface areas with limited vertical extent: a shape that is unfortunate when considering its possible environmental consequences. The importance of the density difference between the release gas and the environment depends strongly upon the volume of release or the release rate and the ambient wind speed [3].

1.1 Background

Considerable effort has been expended over the last few years investigating the structure of dense gas clouds and plumes in idealized flat terrain [4], and our understanding of these flows has markedly improved. There is still much to do, however, in the development and testing of efficient numerical codes that correctly incorporate the relevant physics, in determining the limitations and advantages of fluid modeling, and in obtaining and analyzing field data. In addition, it must be recognized that the eventual user of this knowledge (attempting, for example, a risk assessment study) must consider the far more complicated problems of incorporating real terrain and local obstacles, and, as a result, has sought more effort in these areas ([4], p. 247).

Common sense suggests that topography, in the form of ground slope, isolated hills or more complex terrain, will alter or divert the cloud or plume. The topography may enhance plume dilution and divert the plume away from regions of elevated terrain. Alternately, the dense plume may be channeled into valleys or low-lying areas and be protected there from the diluting influence of the ambient flow.

The importance of the terrain slope is particularly apparent when the wind speed is insignificant. Entrainment theory can be applied to two-dimensional sources on two-dimensional slopes [5]. Observations support the predictions that entrainment into the plume and subsequent plume dilution increases with slope in a manner so as to ensure that the plume velocity is independent of distance down the slope and very nearly independent of the value of the slope. Similar results also hold for the starting plume [6], and the downslope velocities are generally about $U_p \cong (g_o' q_o)^{1/3}$, where $g_o' = g(\rho_o/\rho_a - 1)$, ρ_o is the source density, ρ_a the ambient density, and q_o the volume flow rate of source material per unit width across the slope. An alternative formulation of this result that will prove useful later is $U_p \cong (g_m' \bar{z})^{1/2}$, where $g_m' = g(\rho_m/\rho_a - 1)$, ρ_m is the maximum density in the plume, and $\bar{z}$ is the centroid of the density distribution. Two-dimensional instantaneous releases on two-dimensional slopes have downslope flows that decrease with time or distance [7]. Point-source releases

on slopes have received less attention, although Feitz [8] undertook a variety of laboratory experiments and found difficulty in obtaining a fully turbulent plume. In all these cases, slopes of 5° or larger were used, since smaller slopes led to laminar or laminar-like plumes.

Ellison and Turner [5] also considered the two-dimensional plume/two-dimensional slope problem with a moving ambient and found agreement between their observations and application of an entrainment theory. They were able to show that an ambient upslope velocity of 2 to 3 times the plume downslope velocity (with no ambient velocity), U_p, would lead to an upslope plume flow. However, they stressed that their analysis is only valid when the moving ambient is non-turbulent and either opposes the buoyancy-driven motion or, if they are in the same direction, the ambient flow is smaller than the buoyancy-driven flow. Under some weak conditions, the solution is such that the ambient velocity is merely added to U_p. Dilution of the plume is reduced by a factor of $U_p/(U_p+U_a)$ for a downslope ambient velocity U_a, and increased by the same factor for an upslope ambient flow.

These observations are of limited use in many atmospheric dispersion problems where the buoyant plume is also being altered by a turbulent boundary layer. Hall et al. [9] extended a study of dense gas plumes to include cases where a continuous plume was released on a 1:12 ramp. With ambient flow down the slope, the plume was narrower than that on a flat surface; alternately, the plume advanced down the slope against an upslope ambient flow until it reached the ramp bottom. It then widened considerably before being carried up the slope. In the absence of the slope, the plume width at the source was about 1 m. A two-dimensional release confined to this width would produce a downslope flow U_p of about 0.35 m/s with no ambient flow. This is only a little smaller than the reference velocity used in the experiment; the strong influence of slope is not surprising. However, little information is available and these early experiments may have had laminar-like flows.

In an analysis taking account of a turbulent, ambient flow, Fay and Ranck [10] suggested that terrain effects were of consequence when $u_*^2/g_m'\bar{z} << \Theta$, where u_* is the friction velocity (of the ambient flow) and Θ is the (small) slope in radians. They found that an upslope flow would be retarded (with an increased dilution), whereas the downslope flow would have a larger velocity (with a decreased dilution). These results are similar to those of Ellison and Turner [5].

Some of the field experiments with instantaneous releases at Porton Down [11] showed evidence of slope influence; however, the interpretation of these transient experiments will not be attempted here. The Burro 8 field experiment [12] may have been influenced by terrain, since $u_*^2/g_m'\bar{z}$ was smaller than the slope near the source. However, specific conclusions are not easily drawn. The unusual, bifurcated plume development of that test did not reflect local topography.

1.2 Goals

The current study had two main goals. The first was to measure in detail a particular dense gas plume and thereby increase our understanding of such plumes. It was not intended to physically model any particular situation. What was intended was to study a dense gas plume in a deep turbulent boundary layer under conditions in which molecular effects were insignificant (e.g., large Reynolds and Peclet numbers) and the negative buoyancy was of significance in determining the plume structure. A physically large plume was also a requirement to enable detailed investigation of the plume structure. That is, no modeling assumptions and/or approximations were to be made over and above those required in the case of a neutrally buoyant plume. We consider later what limitations our observations on dense-plume structure place on fluid modeling and the approximations used to extend modeling results by allowing distortions.

Specific physical modeling aside, laboratory experiments provide well-controlled, inexpensive and quick results that aid in the development and verification of numerical models. Of course, it is essential that the numerical model correctly contain all the relevant physics of the problem and that the laboratory experiment adequately tests the modeling of the relevant physics.

The second, more novel, goal was to observe and quantify the interaction of a dense-gas plume with a simple terrain feature. With these goals in mind the following experiment was devised.

1.3 The experiments

The experiment investigated the basic nature of the transport and dispersion of a dense gas plume in a simulated neutral atmospheric boundary layer, both in flat terrain and over a ramp with nominal slope of 14°. This was a natural extension of previous work at the Fluid Modeling Facility, utilizing knowledge gained from projects on (1) the boundary layer structure and dispersion of neutral plumes from ground-level and elevated sources in a simulated neutral atmospheric boundary layer [13,14], (2) the flow structure and dispersion of neutral plumes from ground-level and elevated point sources upwind of a 14° ramp followed by an elevated plateau [15], (3) the structure of turbulence and dispersion in stably stratified fluids [16] and (4) the flow of stably stratified fluids around isolated hills of simple geometry [17].

The new addition in the current work was, of course, the dense gas; the excess density was obtained using carbon dioxide (CO_2) which, with molecular weight of 44, is 52% heavier than air. The plume was tracked by mixing a small fraction (3% by volume) of ethane (C_2H_6) with the CO_2 and using flame ionization detectors (FIDs) to measure concentrations downstream.

We were aware that the stabilizing effect of the density gradient could effect a laminarization of the plume, a problem we believe renders some laboratory studies unrealistic (hence, should be avoided). The first exercise, therefore,

was a flow visualization study wherein the same mass flux of CO_2 was used in the source as was to be used in the later quantitative studies, and smoke was injected into it to make the plume visible. This plume was observed (and photographed) at several wind speeds to ascertain whether its basic character was laminar or turbulent. The lowest wind speed at which the plume appeared fully turbulent was approximately 1 m/s, and this wind speed was thus used for the quantitative tests conducted later. With this wind speed, the Reynolds number based on the size of the roughness elements, ku_*/ν, was about 20, which is only marginal in producing an aerodynamically rough-wall flow [18].

The work is most easily described by dividing it into three phases. In each of the phases, both neutral and dense gases were emitted into the stream from the source, and the resulting plumes were characterized through concentration measurements made downstream: longitudinal, lateral and vertical profiles at several locations for each plume. In Phase I, the terrain was flat, consisting only of the roughness panels used to generate the boundary layer. In Phase II, the 14° ramp was placed with base (beginning of upward slope) approximately 1800 mm downwind of the source. In Phase III, the same ramp was placed with base approximately 600 mm downwind of the source. Because of the necessarily large mass flux but desired small efflux velocity (to avoid rapid initial dilution and so complicate the problem further), an area source was used instead of the point source used in previous studies. An area source is typical of many release scenarios postulated. Many releases, specific in type very close to the source, might at some short distance downwind be considered an area source of some new volume flow rate and new initial density.

2. Experimental arrangements

The experimental work was conducted in the EPA Fluid Modeling Facility's Meteorological Wind Tunnel, which has a test section 3.7 m wide, 2.1 m high and 18.3 m long, and is described in detail by Snyder [19]. A simulated neutral atmospheric boundary layer was developed using a 153 mm high fence just downstrean (65 cm) of the entrance to the test section and gravel roughness (10 mm) covering the entire floor downstream of the fence. This arrangement was similar but not identical to that described by Castro and Snyder [13] and Snyder and Britter [14]; because of the much lower wind speed in the current study (1 m/s rather than 4 m/s), a honeycomb was used at the exit of the contraction to provide better uniformity and stability of the flow. The ceiling height was adjusted in accordance with previous measurements made with similar geometry (but at a free-stream wind speed of 4 m/s) to reduce variations in free-stream speed to less than 2%.

Extensive measurements of the boundary-layer structure at 4 m/s were made by Snyder and Britter [14] and Castro and Snyder [13]. Because of the difficulties of using hot-wire anemometry at the very low wind speeds, only lim-

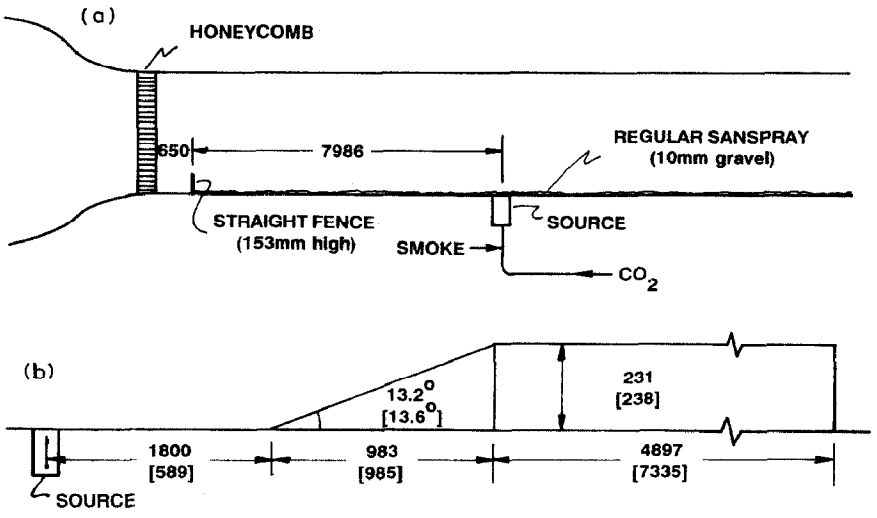

Fig. 1. Configuration of the test section, source, and ramps. All dimensions in mm. (a) Basic flat-terrain setup; (b) Ramp installations. Phase III dimensions shown in square brackets.

ited measurements (mean velocity and longitudinal velocity fluctuations) were made at 1 m/s using a pulsed-wire anemometer [20]. Measurements of the dispersive characteristics were also made at the wind speed of 1 m/s and compared with those taken at 4 m/s. Both of these sets of comparisons showed that the boundary layer was essentially independent of Reynolds number, even at 1 m/s.

The "source" consisted of a metal cylinder (104 mm diameter) filled with gravel through which the source gas flowed. The top of the cylinder was flush with the floor of the test section, and the gravel was spread such as to maintain a homogeneous surface roughness across the entire floor of the tunnel, including the source itself. The effluent was thus effectively uniform over a circular area of 104 mm diameter. The efflux velocity was approximately 6 cm/s, slightly larger than the friction velocity u_* (4.8 cm/s) at the free-stream speed of 1 m/s.

In the flat-terrain tests, of course, the tunnel floor was flat and covered with gravel roughness. In the second phase, a ramp was installed with base (beginning of slope) at a distance of 1800 mm downwind of the center of the source. The slope of the ramp was 14°, or 1:4 (in actual construction, the slope was slightly smaller, as shown in Fig. 1). An elevated plateau extended 4.9 m downwind of the top of the ramp. The ramp and the plateau were covered with the same gravel roughness as the flat terrain. In the third phase, the ramp was moved closer to the source, with base 600 mm from the source center. The elevated plateau extended, in this case, 7.3 m downwind of the top of the ramp. The configuration of the test section, source, and models is shown in Fig. 1.

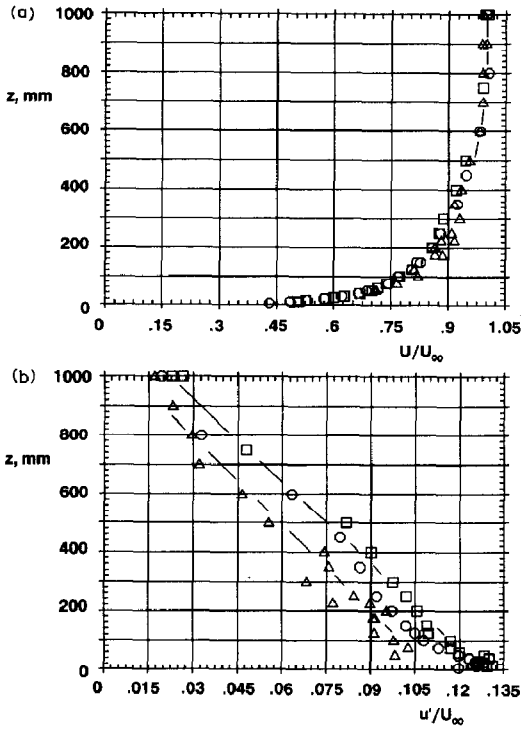

Fig. 2. Flow structure at source position with free-stream wind speeds of 1 m/s (△) and 4 m/s (□,○). (a) Mean velocity profiles; (b) Longitudinal turbulence intensity profiles.

Ethane was used as the tracer gas in these experiments, and flame ionization detectors (FIDs) were used to measure the concentrations. Except for a few cases (where the tunnel wind speed was quadrupled or when measurements were to be made very close to the source), the ethane flow rate was maintained at 900 cc/min. Similarly, air for the neutral plume studies or carbon dioxide for the dense plume studies was maintained at the rate of 30,000 cc/min. The FIDs were calibrated in accordance with standard procedures [21] using ethane/air mixtures; the response of the FIDs to ethane/carbon dioxide/air was investigated separately.

As mentioned above, the volume ratio of ethane to carbon dioxide in the dense gas mixture at the source was maintained constant (at 0.0291 pts C_2H_6/pts CO_2). In this separate series of tests, this "source" mixture was diluted with known amounts of air, and the resulting mixtures were sampled by the FIDs. The FIDs (having been calibrated with ethane/air mixtures) indicated consistently larger values of ethane than actually existed, presumably because of the presence of the CO_2; the ratio of actual to indicated concentration was 0.902 ± 0.024 over the range of source-gas dilutions of 5 to 300. All concentrations shown herein have been corrected in accordance with these

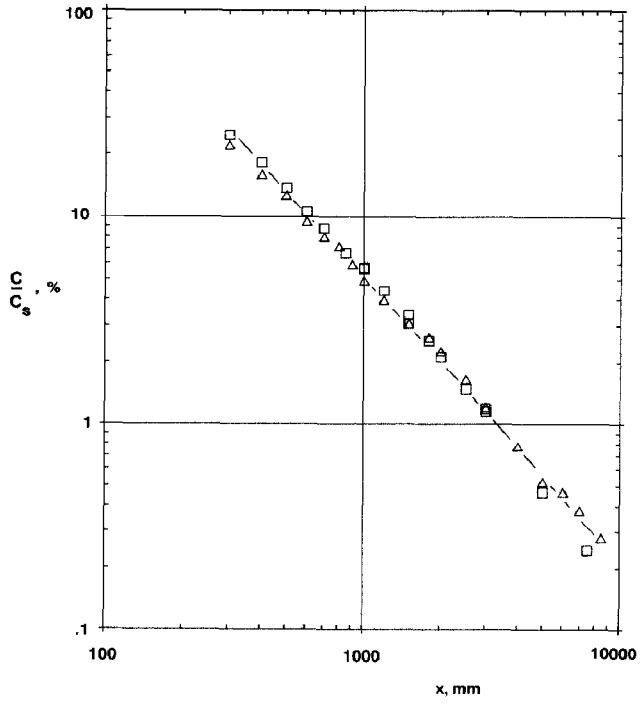

Fig. 3. Comparison of longitudinal surface concentration profiles from a neutrally buoyant source with free-stream wind speeds of 1 m/s (△) and 4 m/s (□).

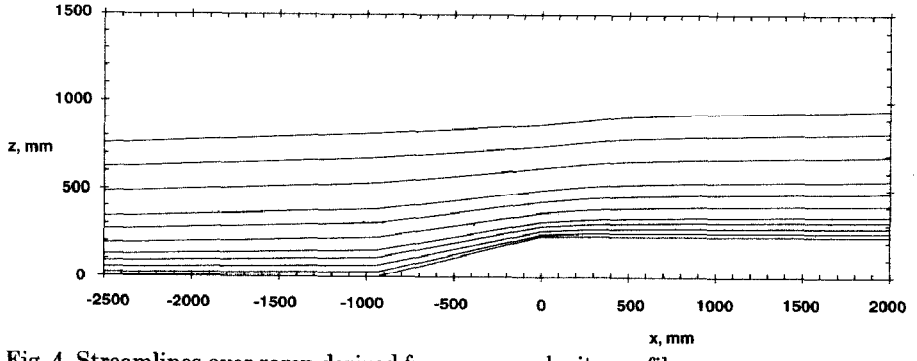

Fig. 4. Streamlines over ramp derived from mean velocity profiles.

findings, and are reported as fractions of source concentration, i.e., C/C_s in percent by volume.

The outputs of the FIDs were sampled using a microcomputer with a Data Translation A/D converter. The sampling rate was 20 samples/s, although the response time of the FIDs was much slower, approximately 1 s. The sampling duration was 2 min. Because of the small wind speed and the relatively small averaging time, the scatter in the concentration data is somewhat larger than is usually observed.

3. Presentation of results

3.1 Boundary layer structure

The simulated atmospheric boundary layer at $U_\infty = 4$ to 8 m/s has good lateral homogeneity and develops slowly between 8 m and 18 m downstream from the fence. It has a boundary layer thickness δ of about 800 mm, and measurements at 8 m downstream from the fence produced a roughness length $z_0 = 0.13$ mm and a friction velocity of $u_*/U_\infty = 0.048$ [13]. The mean velocity and longitudinal turbulent velocity profiles are reproduced in Fig. 2, where both variables are non-dimensionalized with the free-stream velocity U_∞. The near-wall ratios u'/u_*, v'/u_* and w'/u_* are 2.6, 1.8 and 1.3, where u', v' and w' are the r.m.s. longitudinal, lateral and vertical velocity fluctuations, respectively.

Velocity measurements at a nominal free-stream velocity of 1 m/s were made in an earlier independent study with a pulsed-wire anemometer; these are also shown in Fig. 2. From the figure, it is evident that a slightly smaller boundary layer thickness of 700 mm is more appropriate at the smaller wind speed. There is also an apparent reduction of the longitudinal velocity fluctuations by about 10%. The profile of mean velocity was well fitted by the near-wall logarithmic law using the same z_0 of 0.13 mm as was obtained with $U_\infty = 4$ m/s and a friction velocity deduced such that $u_*/U_\infty = 0.048$. A check on the free-stream velocity was obtained by timing smoke puffs as they passed through the tunnel outside the boundary layer. The deduced velocity of 0.95 ± 0.02 m/s was taken as the free-stream velocity in the subsequent quantitative measurements.

To further document any variations of the boundary layer structure with free-stream velocity, profiles of the mean concentration at ground level (actually, $z = 5$ mm) with free-stream velocity and source flow rate increased by factors of 4 were compared with those with a nominal free-stream velocity of 1 m/s. The comparison of ground-level concentrations along the centerline (Fig. 3) does show some variation with free-stream velocity; however, the differences are small and comparable with those expected from the random variations of concentration resulting from the limited averaging time. Lateral and vertical profiles at $x = 2500$ mm both showed small reductions in plume dimensions at the smaller velocity, by 3% in σ_y and 6% in $\bar{z}$; both these values are comparable with the experimental repeatability.

3.2 Flow structure over the ramp

An earlier investigation (unpublished though partially reported by Thompson and Snyder [15] used the same boundary layer (but with $U_\infty = 4$ m/s) and addressed the flow over the ramp and dispersion from point sources upstream of the ramp. The streamline pattern over the ramp (Fig. 4) shows a deceleration of the flow upstream of the ramp base and a subsequent acceleration to the ramp top. The mean velocity at a fixed height above the surface, $z/h = 0.2$ ($z = 50$ mm) for example, was reduced by 40% at the ramp base and

increased by 50% at the ramp top. Mean velocities measured on a given streamline would show slightly smaller changes. Only small changes in the absolute magnitudes of the three turbulence components were noted. The turbulent velocities (again at $z/h=0.2$) were altered by +10% (u'), −10% (v') and 0% (w') at the base of the ramp, and by −10% (u'), −10% (v') and +20% (w') at the top of the ramp.

3.3 Flow visualization

Flow visualization was done prior to the collection of quantitative data to obtain a quick idea of the effects of wind speed and of the terrain, and to ascertain the conditions under which plume laminarization would occur. One video and three still cameras were set up to provide various views of the plumes. The source geometry was as described earlier, and pure CO_2 was emitted from the source at the rate of 30,000 cc/min. Mineral oil was vaporized directly into the CO_2 stream to make the plume visible; previous experience suggests that smoke added in this manner does not significantly alter the density of the source gas.

Photographs were taken of the plumes over both flat terrain and over the ramp (Phase II), at nominal free-stream wind speeds of 4, 2, 1, 0.75, and 0.50 m/s. Some of these are shown in Fig. 5. At wind speeds of 2 and 4 m/s, no density effects were obvious, as the visual plumes appeared identical at the two wind speeds. At 1 m/s, the negative buoyancy of the plume was quite evident, as the visual plume was about 1000 mm wide at $x=1800$ mm. Strong density effects and some plume laminarization were seen at $U_\infty=0.75$ m/s. The plume was clearly laminar at $U_\infty=0.5$ m/s (Fig. 6). The ramp appeared to cause a significantly wider visual plume (Fig. 5); estimates from the photographs suggested 30% wider visual plumes at both wind speeds.

3.4 The plumes in flat terrain

Despite the different plume shapes seen in the flow visualization, the ground-level concentrations downstream from the source on the centerline are strikingly similar when the neutral and dense plumes are compared (Fig. 7). The neutral plume concentration decreases with x as a power law with an exponent of about −1 until $x\cong 1000$ mm, whereafter an exponent of −1.5 is more appropriate. The latter exponent is typical of laboratory data [14]. Close to the source, the finite source size, in particular the finite source width, produced a slower decay rate, more typical of a line source; hence, the −1 slope.

For the neutral plumes, the lateral profiles of ground-level concentration had Gaussian forms, even very close to the source (Fig. 8). For example, at $x=300$ mm (about 3 source diameters), the skewness of the profile was 0.001 and the kurtosis was 2.97. This reflected the visual observations of an initially "compact plume" with a lateral dimension similar to the source size undergoing considerable meander. The plumes at $x=5000$ and 8500 mm were offset

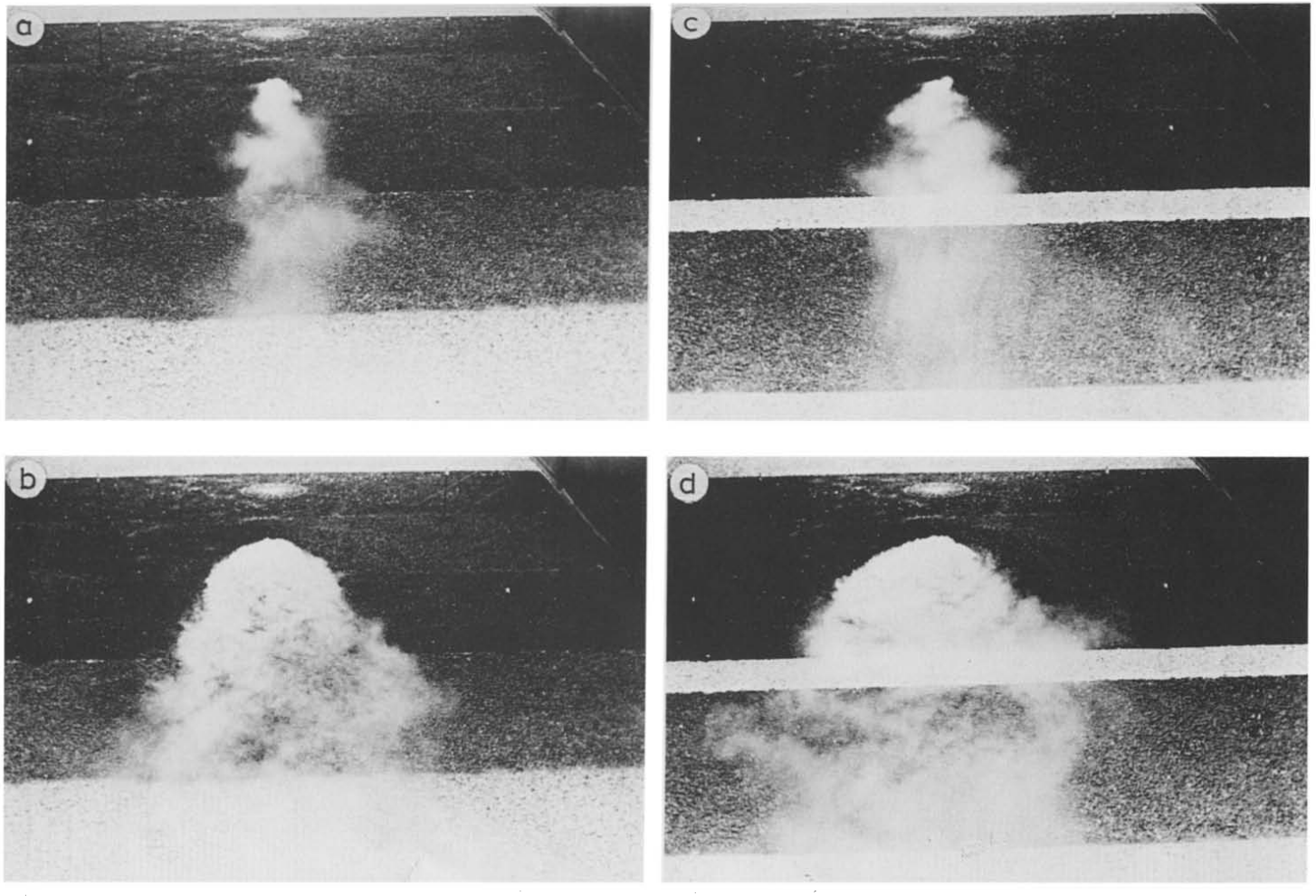

Fig. 5. Visualization of lumes over flat terrain and over the ramp with wind speeds of 1 and 2 m/s. The sloped surface is the white band across the middle of the right-hand photographs. (a) Flat terrain, $U_\infty = 2$ m/s; (b) Flat terrain, $U_\infty = 1$ m/s; (c) Ramp terrain, $U_\infty = 2$ m/s; (d) Ramp terrain, $U_\infty = 1$ m/s.

Fig. 6. Laminarization of plume over flat terrain at $U_\infty = 0.5$ m/s.

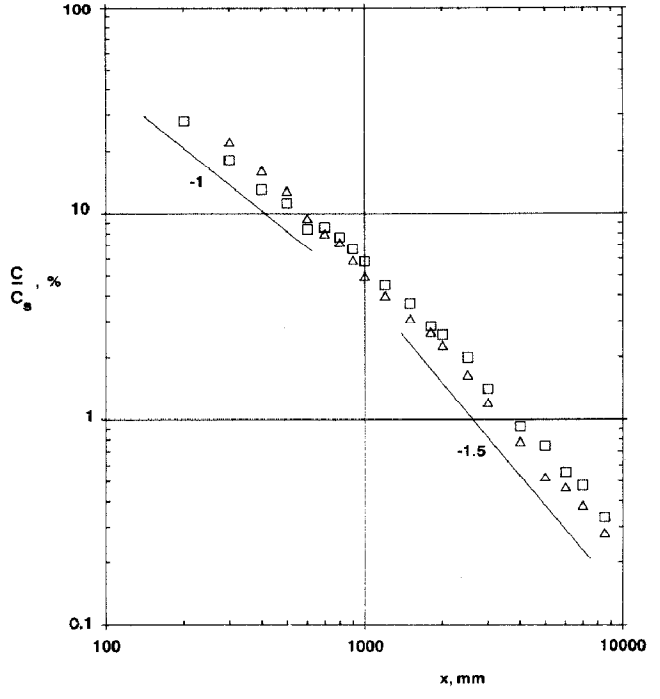

Fig. 7. Comparison of centerline ground-level concentrations downstream from the source for dense (□) and neutral (△) plumes in flat terrain.

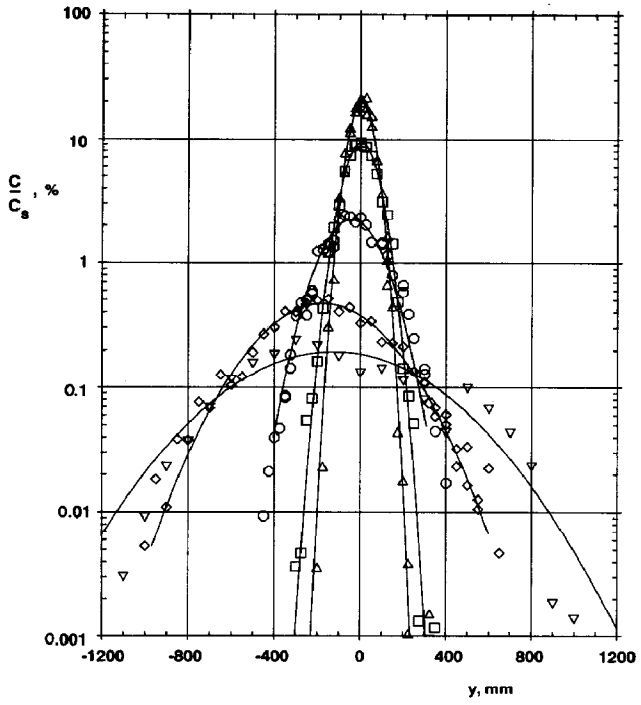

Fig. 8. Crosswind ground-level concentration distributions for the neutral plume at $x=$: △, 300; □, 600; ○, 1800; ◇, 5000; and ▽ 8500 mm downwind of the source in flat terrain. The lines represent best-fit Gaussian curves through the data.

from the tunnel centerline by 173.6 mm and 124.3 mm, respectively, indicating a substantial lateral drift of the plume. A second lateral profile at $x=8500$ mm taken 35 min later produced a plume with σ_y smaller by 4% and an offset of only 3.56 mm. The difference in σ_y reflects the level of repeatability in σ_y and σ_z throughout the study, while the substantially different offset indicates the possibility of very slow changes in the mean flow pattern in the tunnel. Considerably smaller offsets were more normally encountered.

The vertical concentration profiles for the neutral plume (Fig. 9) were not Gaussian, but were similar to those obtained from point sources at ground level [22]. Their shapes may be described as a vertical variation of the form $C/C_{mx}=\exp(-Az^n)$, with $n\cong 1.5$.

The dense plume, although producing a longitudinal decay of ground-level concentration much the same as the neutral plume, had distinctly different shapes of lateral and vetical profiles. The lateral profiles of ground-level concentration (Fig. 10) were very flat-topped with sharp tails, although the sharpness was less obvious at large distances from the source. The buoyancy-induced lateral spreading provided both the lateral uniformity of concentration and the sharpness of the lateral edge of the plume, resulting in a kurtosis which was

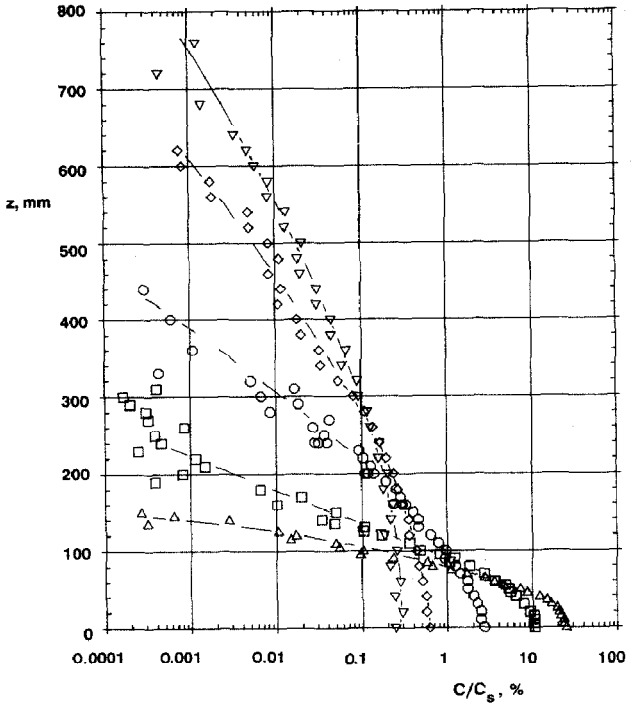

Fig. 9. Vertical concentration distributions for the neutral plume at $x=$: △, 300; □, 600; ○, 1800; ◇, 5000; and ▽, 8500 mm downwind of the source in flat terrain.

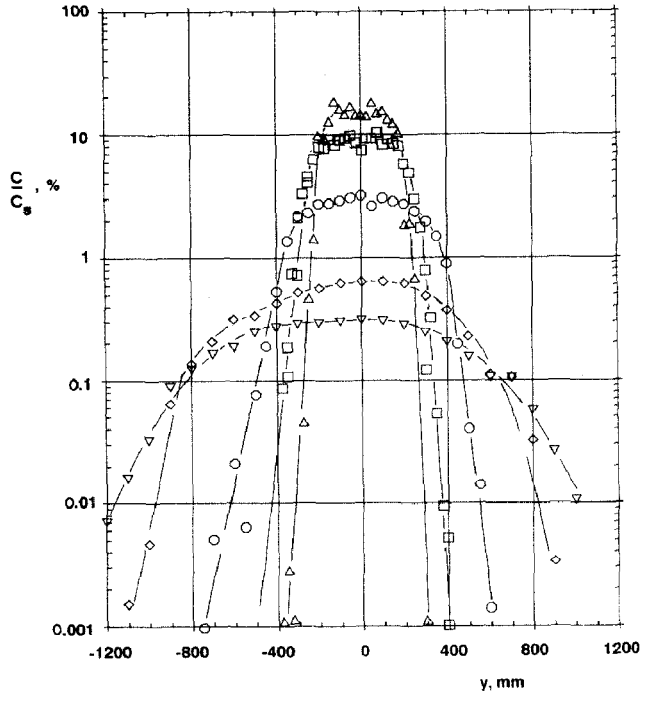

Fig. 10. Crosswind ground-level concentration distributions for the dense plume at $x=$: △, 300; □, 600; ○, 1800; ◇, 5000; and ▽, 8500 mm downwind of the source in flat terrain.

2.0 at $x=300$ mm and 2.45 at $x=5000$ mm. A considerably longer fetch would be required to regain the Gaussian kurtosis of 3. A lateral profile taken at the position of the source center (and $z=0$ mm) indicated a plume that was considerably wider than the physical source size, with a σ_y of 53.7 mm. Note that a top-hat profile over -52 mm $<y<52$ mm has a σ_y of $52/\sqrt{3}=30.0$ mm. Another lateral profile at the downstream edge of the source ($x=52$ mm; $z=5$ mm) showed a similar σ_y of 56.4 mm.

The vertical concentration profiles for the dense plume appear nearly linear when plotted on log–linear axes (Fig. 11), particularly for $x<2500$ mm. This variation may be written as $C/C_{mx}=\exp(-z/\bar{z})$, where C_{mx} is the ground-level (or maximum) concentration and $\bar{z}$ is the centroid of the concentration distribution. The skewness and kurtosis about $z=0$ are typically 2.4 and 6.0 compared with values of 1.7 and 2.25 for the neutral plume. The cause of the nearly exponential decrease of concentration with height in this buoyancy influenced, laterally diverging plume is obscure and possibly fortuitous. However, the profiles are substantially different from those of neutral plumes.

We have characterized the lateral profiles with their standard deviation σ_y, and the vertical profiles with their centroid, $\bar{z}$. The lateral plume width σ_y (Fig. 12) increased very rapidly with x when the plume was dense compared with the development of the neutral plume The difference in the growth rate is most marked close to the source; it is insignificant for $x>5000$ mm, although it should be stressed that even then the lateral profile shapes are distinctly different from those of the neutral plumes.

The centroid $\bar{z}$ of the vertical profiles is markedly reduced in the dense plume (Fig. 13) and the difference in $\bar{z}$ between the dense and neutral plumes continues to increase over the entire measurement region. Thus, over the measurement region, the plume is always influenced by the plume buoyancy. Similar observations were made for σ_z (about $\bar{z}$) as for $\bar{z}$.

3.5 The plumes over the ramp at x$=1800$ *mm*

For the neutral plume, the ramp had little influence on the ground-level concentration on the centerline for $x<1500$ mm (Fig. 14). At the base of the ramp ($x=1800$ mm), there was a reduction in ground-level concentration of about 20%. The reduction was about 25% by the top of the ramp and this reduction was maintained out to $x=7500$ mm.

The results for the dense-gas plume (also Fig. 14) were superficially similar. A smaller reduction of the ground-level concentration was observed at the ramp base, but by the top of the ramp, the reduction was 30% and this was subsequently maintained out to $x=7500$ mm.

None of the vertical or lateral profiles of mean concentration had any significant changes in shape due to the ramp, either qualitatively or quantitatively, as measured by the skewness or kurtosis. As a consequence, the plume statistics are usefully described by σ_y and $\bar{z}$. For the neutral plume, σ_y was increased near the base of the ramp (Fig. 15). The dense plume underwent similar widening at the base of the ramp (Fig. 16), and a subsequent reduction

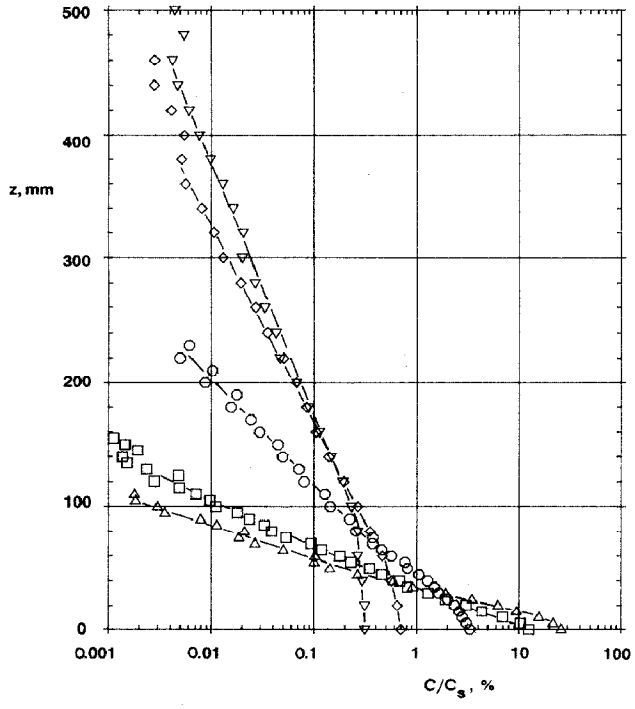

Fig. 11. Vertical concentration distributions for the dense plume at x=: △, 300; □, 500; ○, 1800; ◇, 5000; and ▽, 8500 mm downwind of the source in flat terrain.

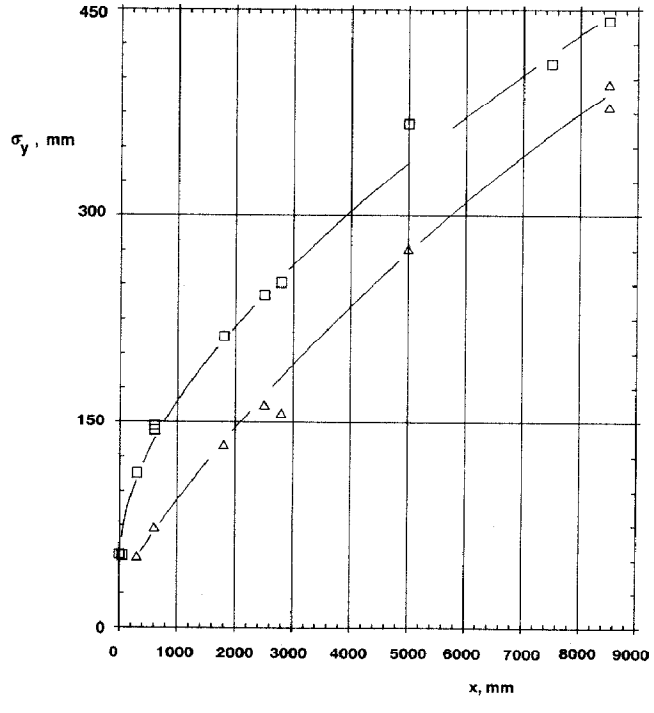

Fig. 12. Comparison of lateral widths of neutral (△) and dense (□) plumes in flat terrain.

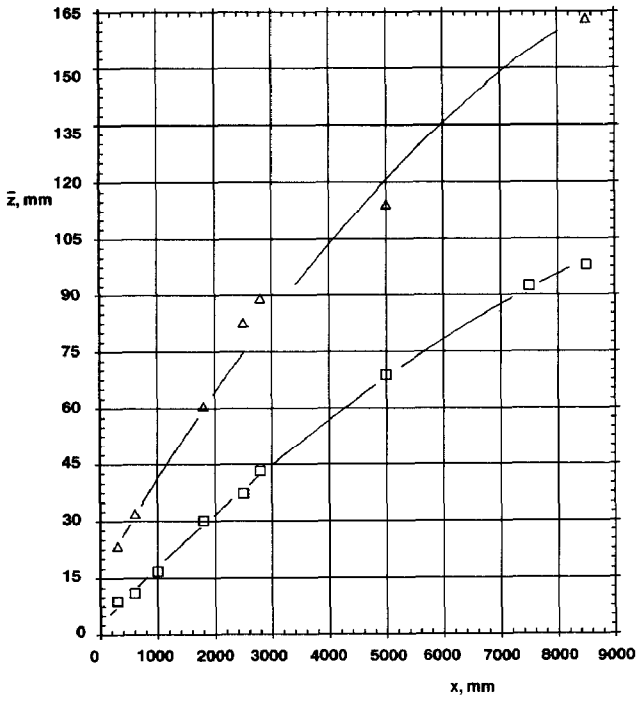

Fig. 13. Comparison of centroids of concentration distributions of neutral (△) and dense (□) plumes in flat terrain.

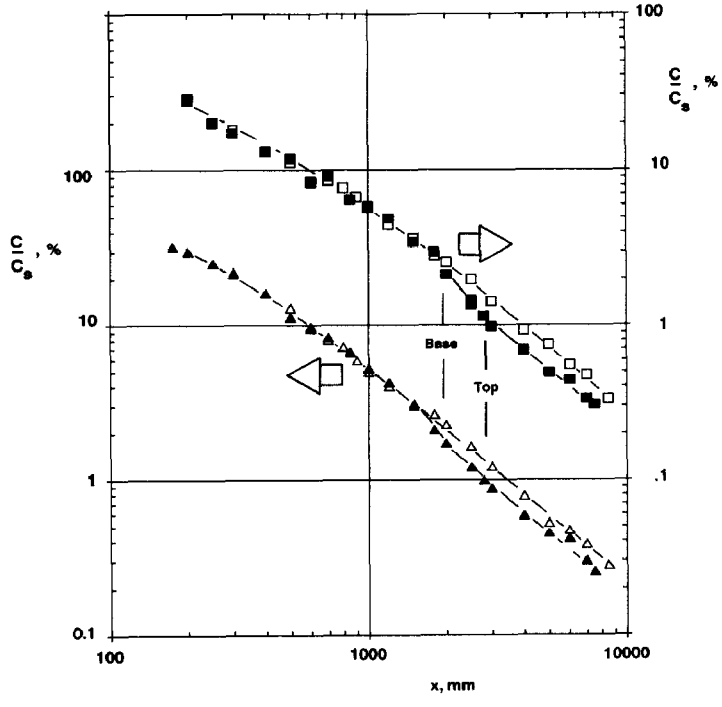

Fig. 14. Comparisons of surface longitudinal concentration distributions for neutral (△) and dense (□) plumes in flat terrain (open symbols) and over ramp (filled symbols). Phase II: ramp begins 1800 mm downwind of source.

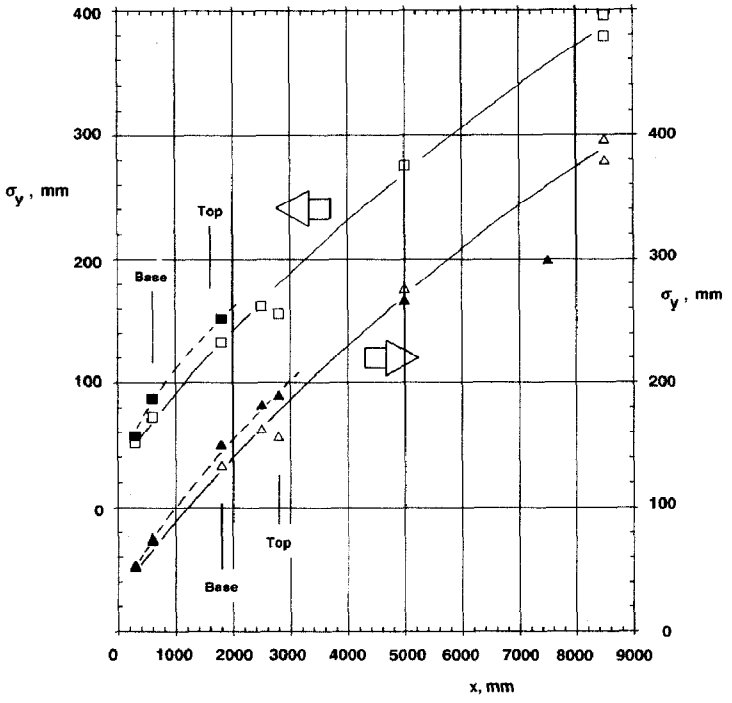

Fig. 15. Comparison of neutral plume widths in flat terrain (open symbols), over the ramp at 600 mm (■), and over the ramp at 1800 mm (▲).

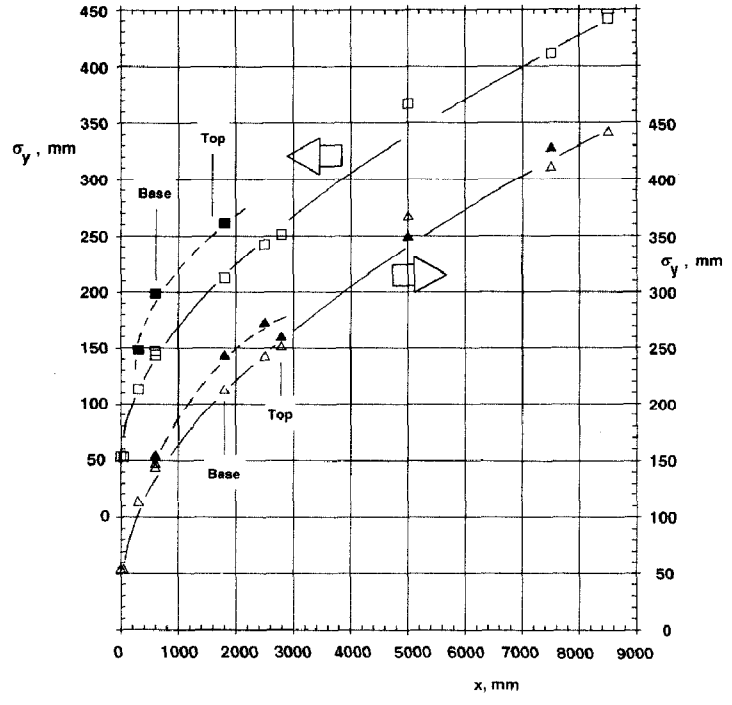

Fig. 16. Comparison of dense plume widths in flat terrain (open symbols), over the ramp at 600 mm (■), and over the ramp at 1800 mm (▲).

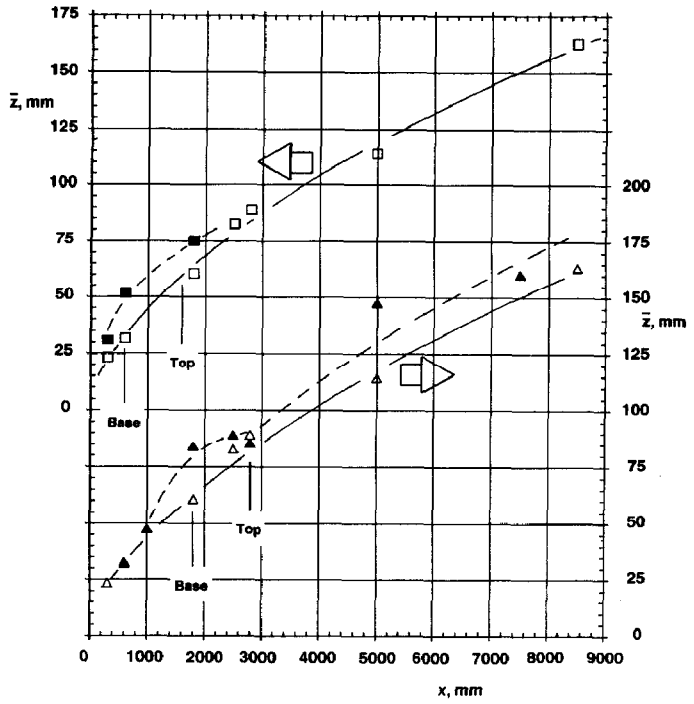

Fig. 17. Comparison of neutral plume centroids in flat terrain (open symbols), over the ramp at 600 mm (■), and over the ramp at 1800 mm (▲).

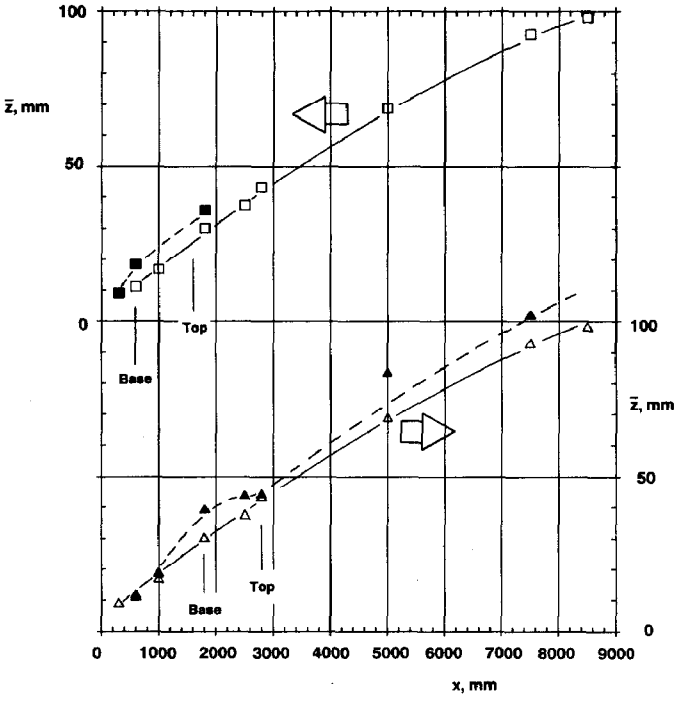

Fig. 18. Comparison of dense plume centroids in flat terrain (open symbols), over the ramp at 600 mm (■), and over the ramp at 1800 mm (▲).

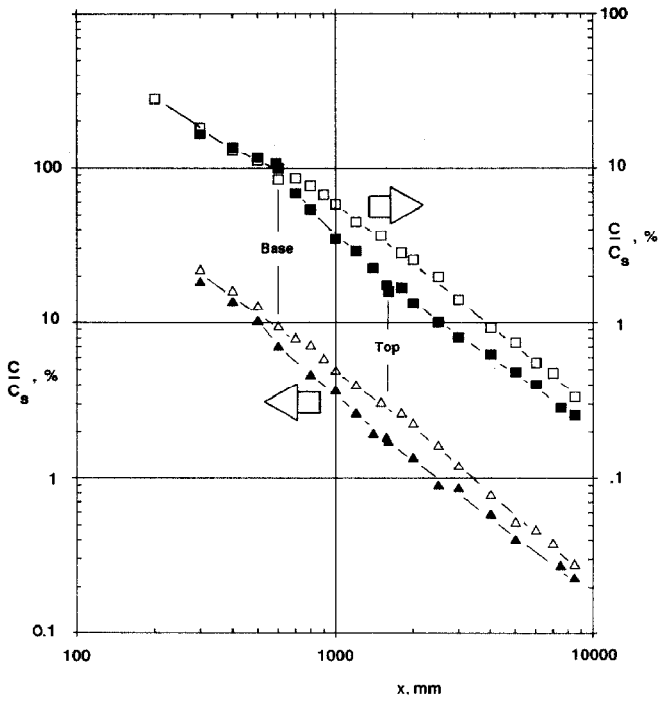

Fig. 19. Comparisons of surface longitudinal concentration distributions for neutral (△) and dense (□) plumes in flat terrain (open symbols), and over ramp (filled symbols). Phase III: ramp begins 600 mm downwind of source.

in widening as the plume was transported up the slopes, although the effects were small and experimental scatter clouds the interpretation.

The effects on the neutral plume depth as measured by $\bar{z}$ (Fig. 17) were larger than those on σ_y, a result of $\bar{z}$ increasing with streamline divergence and also any changes in the turbulent diffusion, whereas σ_y is only altered by changes in turbulent diffusion. The streamline contraction near the ramp top is also apparent. Farther downstream, the plume depth remained larger than that in the absence of the terrain (unlike the changes in σ_y). For the dense plume (Fig. 18), similar (but smaller) variations in $\bar{z}$ were observed.

Quantitatively, the changes in σ_z about $\bar{z}$ were the same as those in $\bar{z}$, a further indication that the plume shapes were not altered significantly.

3.6 The plumes over the ramp at x = *600 mm*

The distance from the source to the ramp base was decreased to a nominal 600 mm, with the ramp top at $x = 1574$ mm. With a neutral plume, the ground-level concentrations on the centerline were reduced slightly by the ramp at $x = 300$ mm, and by about 30% at the ramp base (Fig. 19). The reduction was

about 50% at the ramp crest. The difference in ground-level concentration between the flat terrain and the ramp terrain became smaller farther downwind.

The plume width, σ_y (Fig. 15), and centroid, $\bar{z}$ (Fig. 17), were both increased at $x=300$ mm and substantially increased at the ramp base. The σ_y increase was maintained as the plume traveled to the top of the ramp. The plume centroid grew more slowly over the ramp as the streamlines contracted near the ramp top. Note that the comparison has been made at 1800 mm rather than at the ramp top (1574 mm); the longitudinal profiles indicate that such a comparison is representative of a comparison at the ramp top.

With the distance between source and ramp reduced to a nominal 600 mm, the dense plume was more stable at the position of the ramp base than when the ramp base was at $x=1800$ mm. The ratio of plume thickness to ramp height was also reduced in this case. A stronger interaction between the plume and the ramp was therefore anticipated.

At $x=300$ mm (see Figs. 16, 18 and 19), the plume was wider by 30%, with no change in $\bar{z}$ or the maximum ground-level concentration. The width increased by 37% at the ramp base and $\bar{z}$ increased by 56%, but the ground-level concentration was virtually unchanged. The lateral plume width increase was maintained to the ramp top, while the increase in $\bar{z}$ was reduced. The reduction in ground-level concentration (compared with flat terrain) occurred between the ramp base and top. Farther downstream, the difference between the flat and ramp terrain decreased.

4. Discussion

4.1 Flat terrain

In flat terrain the lateral profiles of the dense gas plume displayed very little variation of mean concentration over the central (major) part of the plume. There was no evidence of plume bifurcation at any position and we are confident that previous observations of plume bifurcation are more frequently the result of the flow around an obstacle at the source [23] or from significant vertical momentum in the plume at the source. Even at $x=8500$ mm, the non-Gaussian form of the concentration distribution of this dense gas plume was evident, although this may indicate the considerable distance required to alter a finite length line source to a Gaussian profile rather than the persistance of the buoyancy-driven lateral spreading.

The lateral growth of the plume results from both the boundary layer turbulence and a buoyancy-driven flow. A velocity, characteristic of the growth of the lateral width of the plume as a result of buoyancy, might by estimated from the pressure differential that drives the lateral flow, i.e., $\rho_a \int_0^\infty g' \, dz$ and would be of order $(\int_0^\infty g' \, dz)^{1/2}$. This may be approximated by $(g_m' \bar{z})$, where

TABLE 1

Lateral growth rate of dense gas plume

x, mm	$\frac{\sigma_y-\sigma_{y0}}{L_b^{1/3}x^{2/3}}$	$\frac{\sigma_y-\sigma_{y0}}{\mathscr{L}_b^{1/3}x^{2/3}}$
300	0.918	0.466
600	0.911	0.509
600	0.878	0.490
1800	0.743	0.486
2500	0.709	0.482
2795	0.689	0.480
5000	0.742	0.558
7500	0.645	0.508
8500	0.645	0.512

$g_m' = g(\rho_m/\rho_a - 1)$, ρ_m is the maximum density in the plume and $\bar{z}$ is the vertical height of the plume centroid. The approximation is exact when the vertical profile of density (concentration) is exponential. These velocities are 11, 8.4, 7.0, 6.1, 4.8, 4.1 and 3.9 cm/s at $x=300$, 600, 1800, 2500, 5000, 7500 and 8500 mm, respectively, and these should be compared with the friction velocity u_* of about 5 cm/s. The lateral concentration profiles have sharp edges when $(g_m'\bar{z})^{1/2} >> u_*$ they approach Gaussian shapes when $(g_m'\bar{z})^{1/2} << u_*$. Close to the source (when $(g_m'\bar{z})^{1/2} >> u_*$), the buoyancy-driven flow is dominant and produces near uniform ground-level concentrations within the plume and sharp plume edges. Our results suggest that $(g_m'\bar{z})^{1/2}/u_* \cong 1$ demarcates buoyancy-dominated flows from those dominated by turbulent diffusion (as regards the lateral growth).

The rapid growth of the lateral plume width has been correlated with $L_H = L_{H0} + AL_b^{1/3}x^{2/3}$ [24]. L_H is the visual plume width, L_b a buoyancy length scale, and A is a constant. A less subjective measure of the plume width, σ_y, is used in Table 1 with $L_b = g_o' q_o/U_\infty^3 = 3.02$ mm to form the parameter $(\sigma_y - \sigma_{yo})/L_b^{1/3}x^{2/3}$. This parameter decreases with x (at about $x^{-0.1}$), and we suggest that this is a result of the increase in the relevant advection velocity as the plume increases in depth.

A more appropriate choice for the advection velocity (rather than proportional to U_∞) would then be the velocity at $z=\bar{z}$. No velocity measurements were made within the dense plume. However, if we use the velocity profile obtained in the absence of the plume to form $\mathscr{L}_b$ with $U(z=\bar{z})$, the parameter $(\sigma_y - \sigma_{yo})/\mathscr{L}_b^{1/3}x^{2/3}$ (see Table 1) is 0.50 ± 0.025, with little trend. This correlation is obviously satisfactory, although this is somewhat surprising at large x where the lateral buoyancy-driven flow is becoming less important than turbulent diffusion.

The visual plume width was estimated from photographs to be 200 mm at

the source, 650 mm at $x=600$ mm and 1040 mm at $x=1800$ mm. The ratio of visual plume width to σ_y, in the form $(L_H-L_{H0})/(\sigma_y-\sigma_{y0})$ is 4.9 at $x=600$ mm and 5.3 at $x=1800$ mm. At the two downstream positions, the visually determined plume edges are at a concentration about two orders of magnitude below the maximum concentration in the profile. In the absence of more data, we use 5.0 as a general conversion factor between the quantitative results and those from the visualization to obtain $L_H=L_{H0}+2.5\mathscr{L}_b^{1/3}x^{2/3}$, where $\mathscr{L}_b=g_o'q_o/U^3(z=\bar{z})$.

The buoyancy-determined lateral plume growth rate of $x^{2/3}$ appears to hold out to a distance in excess of 2800 L_b. This is smaller than the value of 10^4 L_b suggested by Britter [24]. However, these early data were taken in a water-channel study without surface roughness. Alternatively, the plume growth rate was about the same as the growth rate for the neutral plume after about 10^3 L_b. Thus, although the largest of these values might be correct, the use of the smallest may not lead to significant error.

In the present study, $L_b/D=2.9\times10^{-2}$, which is not large enough for L_b to dominate the physical source size, D, nor small enough for the source size to render the plume effectively passive from the source [24]. Thus, both L_b and D will determine the very near source development of the plume.

The increased lateral width of the plume (over the source size) was 32 L_b or 4.6 $\mathscr{L}_b'$ with $\mathscr{L}_b'$ based on the arbitrary choice of the velocity at $z=10$ mm. Similarly, the upstream extent of the plume (past the source edge) was about 20 mm or 6.6 L_b or 1.0 $\mathscr{L}_b'$. It is apparent that, when the upstream plume extent and the lateral width at the source are correlated with the buoyancy length scale, the sensitivity of the buoyancy length scale to the velocity leads to great difficulty in determining a useful and relevant reference velocity.

The shapes of the vertical concentration profiles of the dense gas plumes observed in the experiment were surprising. It is usual, in simplistic model development, to assume a Gaussian profile (or one that is more uniform within the plume) with a sharp upper interface across which entrainment occurs (e.g., see Ref. [25], p. 138). The observed exponential profile was markedly different from either of these assumed forms. The vertical profiles of mean concentration are well fitted by exponential profiles for $x\leq2500$ mm and the fits are reasonable out to $x=8500$ mm. We have no explanation for this particular shape in a laterally diverging flow with vertical density gradients of dynamic significance. However, similar observations were made in the Burro 9 field trials [25].

Our observations indicate that, even at $x=8500$ mm, the vertical plume growth rate is still influenced by the negative buoyancy. If we speculate that the velocity profile is not altered by the dense gas plume, then the local gradient Richardson number is given by

$$Ri = -\frac{(g/\rho)\ (\partial\rho/\partial z)}{(\partial U/\partial z)^2} = \frac{\kappa^2 g_m{}'\bar{z}}{u_*^2}\left\{\left(\frac{z}{\bar{z}}\right)^2 e^{-z/\bar{z}}\right\}$$

which has a maximum of about 0.1 $g_m{}'\bar{z}/u_*^2$ at $z/\bar{z}=2$. κ is von Kàrmàn's constant of 0.4. At $x=8500$ mm, the maximum local gradient Richardson number is 0.07 (using the above estimate): a value large enough to ensure some buoyancy effects. Of course, any change in the velocity profile is, of itself, an indication of a buoyancy influence on the flow. Thus, the vertical growth rate of the plume is still buoyancy influenced at 2800 L_b.

Although the lateral and vertical concentration profiles were dissimilar at various downstream positions, a continuity check was attempted by forming $C_{mx}\bar{z}\sigma_y U(z=\bar{z})/q_o$, where C_{mx} is the maximum concentration at the mid-section. This ratio, evaluated at 7 positions between $x=300$ mm and $x=8500$ mm, had a mean value of 0.227 and a standard deviation of 0.024. Replacing $\bar{z}$ with σ_z (about $z=0$) and multiplying the ratio by 2π gave a mean value of 2.02; a value of 2.0 would be appropriate for a Gaussian plume.

4.2 Ramp terrain

Both ramps produced a reduction in the ground-level concentration of the neutral plume. The plume development was similar in both cases, although more marked in the case with the ramp closer to the source. The changes in mean velocity and consequent transit times of the plume are considerably larger than changes in the absolute magnitude of the turbulence. Our observations are consistent with the expectation of an increased lateral or vertical spread near the ramp base; the former is principally due to an increased time of travel while the latter is also increased by the vertical divergence of the streamlines. The greatest change in ground-level concentration has occurred only a short distance up the ramp. Thereafter, the reduction is maintained over the ramp. Presumably the influence of the ramp (or any topography) will decrease as the plume dimension increases. With the ramp at $x=600$ mm, the height of the plume centroid was 0.14 times the ramp height. The ramp produced smaller effects when at $x=1800$ mm and the height to the plume centroid was 0.26 times the ramp height. Very similar results were obtained for a ground-level point source 1600 mm upstream of the ramp base [15].

Only slight effects of the terrain on the dense gas plume were evident in the first ramp study. The parameter $u_*^2/g_m{}'\bar{z}$ suggested by Fay and Ranck [10] was 0.50 in this case, which is substantially larger than the slope of 0.25. More significant terrain effects were produced in the second study, where $u_*^2/g_m{}'\bar{z}$ was somewhat smaller (0.41). Note that u_* is that of the neutral boundary layer, which may be larger than that under the dense gas plume or near the base of the ramp, but smaller than that at or near the ramp top. Note also that

$g_m' \bar{z}$ was determined at the position of the ramp base in the absence of the ramp.

Unlike the neutral plume, there was little, if any, increased dilution of the plume (caused by the ramp) at the ramp base, although the plume was strongly distorted in the lateral and vertical directions. The reduced mean velocity at the ramp base and consequent increase in plume travel time to reach the ramp base allows greater lateral spreading of the plume. The very small increase in plume dilution may indicate some plume stabilization in this region of decreased velocity shear. Most of the increased plume dilution occurs as the wider plume travels to the top of the ramp. A simple interpretation of this flow is that the lower ambient velocities near the ramp base allow increased lateral spreading and the plume then behaves as if emanating from a line source as it moves to the top.

It was initially surprising that the dense plumes did not widen considerably once on the ramp. However, over much of the ramp, the ambient velocity is increasing toward the top. A change in advection velocity such as this must lead to a reduction in the lateral growth rate of the plume. The criterion developed by Ellison and Turner [5] to reverse a two-dimensional plume on a slope may be reinterpreted (with some approximation) as $u_*^2/g_m' \bar{z} \geq 0.05$; this is only weakly dependent upon slope. In the present experiments, this criterion would only be approached at, or very close to, the source. Britter [26] found that $U_\infty/(g_o' q_o/W)^{1/3}$ and $\bar{z}/H$ were able to correlate the interaction of a dense gas plume from an area source encountering a two-dimensional fence (or 90° ramp). W was the visually determined plume width at the fence position (in its absence) and H was the fence height. Using $W=5\sigma_y$, the parameter $U_\infty/(g_o' q_o/W)^{1/3}$ was 6.2 for the fence at $x=600$ mm and 7.1 for the fence at $x=1800$ mm. The respective height ratios were 0.05 and 0.13. For the same parameters, he found a substantial increase in plume width (greater than a factor of 3) before the plume surmounted the fence. This may be a consequence of the greater velocity reductions (and flow separation) upstream of the fence when compared with the 14° ramp.

It is appropriate now to review what is meant by terrain or slope influence. The two-dimensional experiments of Ellison and Turner [5] were in an inclined channel. The slope, of itself, would not influence the velocity field. Their experiment addressed the direct influence of the plume's negative buoyancy in producing a force down the slope to accelerate or decelerate the plume and the influence of the density stratification on turbulent mixing (entrainment). However, for flow over complex terrain, the terrain changes the mean and turbulent velocity fields. In this ramp experiment, the terrain feature had little direct influence on the dense gas plume; the principal influence was the modification of the velocity field within which the plume was immersed.

Our visualization of the flow at a free-stream velocity of 0.5 m/s, though an unsatisfactory flow with obvious viscous effects, showed a significant direct

influence of the slope on the plume; the plume would not travel up the slope in the along-wind direction.

4.3 Implications for fluid modeling

This study did not model any particular situation, but we may consider the implications of our observations for the modeling of dense gas dispersion.

For both negatively and positively buoyant plumes, fluid modeling of problems that are frequently encountered requires operation of wind tunnels or water channels at very low velocities. This reduction, essentially in the Reynolds number, produces difficulties in maintaining controlled turbulent flows. The very strong density gradients associated with dense gas plumes further act to inhibit turbulence and make the flow even more prone to the influence of Reynolds number. As a result, fluid modeling of a dense gas plume is generally more contentious than a comparable positively buoyant release. A small benefit is that the dense gas plume remains within a region of the boundary layer about which more is known than for the positively buoyant release.

The relevant dimensionless groups for modeling a steady release of a dense gas are $U^2/g_o'L$, q_o/UL^2, ρ_o/ρ_a, various geometrical ratios and boundary conditions and two groups dependent upon fluid properties, the Reynolds number UL/ν and the Peclet number $UL/\mathscr{D}$ (ν is the kinematic viscosity and $\mathscr{D}$ is the mass diffusivity). The complete velocity field is specified in terms of the velocity scale U and length scale L.

Pragmatic fluid modeling relies on the insensitivity of turbulent diffusion and dispersion to the Reynolds and Peclet numbers, *provided* they exceed some critical values. It is, therefore, imperative that any Reynolds number dependence of the flow be minimized; we will show later that this is a more severe constraint than that on the Peclet number. Large Reynolds numbers require large models and large velocities, in conflict with modeling $U^2/g_o'L$ at small scales.

Broadly speaking, an inadequate Reynolds number will make itself obvious by causing the plume to laminarize; it is a contentious point whether a full-scale plume will laminarize if the plume stability is large enough. What we wish to avoid is plume laminarization in a model (assisted by the smaller Reynolds number), when it would not have occurred at a larger scale. A laboratory plume that has laminarized will not model a full-scale plume that is also laminar. Thus observation of a laminar or laminar-like plume in the model negates the validity of the modeling.

If plume entrainment becomes very small in a fluid model, the plume dilution will be influenced by molecular diffusion. To ensure that molecular diffusion is negligible, a large Peclet number must be maintained. As the turbulent diffusion is inhibited by the density gradients in the plume (and turbulent velocities have often been found to vary inversely with a Richardson number [27]), the variables $Pe/Ri = U^3/g'\mathscr{D} \geq 1500$ or $Pe^*/Ri^* = u^3_*/g'\mathscr{D} \geq 0.2$ have

been used to ensure negligible influence of molecular diffusion [28]. This is a reasonable modeling criterion; however, practically, molecular diffusion is unlikely to be of consequence in a model unless the plume has laminarized and the entrainment has fallen to zero. That is, provided the plume is turbulent and not laminar, it is unlikely that any Peclet number criterion will be violated. Similar arguments were put forth by Snyder [18].

The limited velocity measurements available to us and the comparison of the dispersion at $U_\infty = 0.95$ m/s and at a wind speed four times that indicates a rough-wall turbulent boundary layer with little, if any, Reynolds number influence. The source flow rate of 30000 cm^3/min of CO_2 produced a plume that showed significant dense gas behavior, did not appear to be influenced by molecular viscosity or mass diffusivity and was of a vertical and lateral extent that allowed investigation of the plume concentration patterns in detail, over both flat and ramp terrain.

Reduction of the free-stream velocity to a nominal 0.75 m/s led to a slight plume laminarization, while an even greater reduction to 0.5 m/s produced a clear laminarization of the plume. Assuming that the boundary layer was still turbulent (though not necessarily with a fully aerodynamically rough wall), it is apparent that this wind-tunnel plume was strongly influenced by molecular properties and would, therefore, be an inappropriate model of a larger scale flow. Note that this comment is quite separate from the possibility of the strong density gradient inhibiting turbulence in both model and at larger scale, independent of viscosity.

Thus we conclude that the present study with $U_\infty = 0.95$ m/s is a valid model (with no additional uncertainties over those present in the modeling of passive releases) of a dense gas release in an atmospheric boundary layer using $U^2/g'L$, q_o/UL^2 and ρ_o/ρ_a as the modeling parameters. The boundary layer is believed to be Reynolds-number independent.

With a fixed U and L in the model, the boundary layer structure may be internally changed (u_* and z_o) by altering the surface roughness. An increase in the surface roughness presents no difficulties. However, a reduction of surface roughness may lead to a smooth wall boundary layer with $z_o \cong \nu/10\, u_*$. The existence of a viscously dominated sublayer of thickness $10\, \nu/u_*$ must be recognized, and a plume of comparable thickness would not be a valid modelo. Conversion of $U^2/g_0' L\, q_o/UL^2$ and ρ_o/ρ_a to their full-scale values (at a nominal scale ratio of 1:1000) from the present study gives large full-scale velocities and source flow rates. Presuming that any model flow rates less than that used here will produce plumes with reduced influence of their (reduced) negative buoyancy, the required Reynolds number for Reynolds-number independence will be smaller. That is, a turbulent plume is unlikely to laminarize when the source flow rate of dense gas is reduced. The crucial difficulty is the large full-scale-wind speed that is modeled; in this case the full-scale wind speed is $0.95 \times \sqrt{1000} = 30$ m/s at $z = \delta$, and 15.6 m/s at $z = 10$ m.

With our reluctance to reduce the wind tunnel speed below 0.95 m/s, a modeling distortion must be considered and two possibilities are:

(a) *Source density ratio*: Relaxation of the source density ratio ρ_o/ρ_a is valid under the Boussinesq approximation provided $(\rho_o/\rho_a - 1)$ is small compared with unity in model and at full-scale. Neff and Meroney [29] found that experiments with $(\rho_o/\rho_a - 1) = 0.79$ and 1.59 were equivalent, but different from those at 0.22, 0.37 and 0.50. This surprising result was later attributed to molecular diffusion effects [30] at the small wind-tunnel speeds used $(Pe^*/Ri^* \leq 0.2)$. Combining the known correctness of the Boussinesq approximation at small $(\rho_o/\rho_a - 1)$ and the observations by Neff and Meroney [29] (that $(\rho_o/\rho_a - 1) = 0.79$ was equivalent to that for 1.59) gives confidence that the source density ratio may be relaxed over a wide range of $(\rho_o/\rho_a - 1)$. This *may not* be valid for instantaneous releases of height comparable to horizontal dimension; that flow is strongly affected by the initial collapse of the cloud, and the density ratio will be important initially, particularly for large density differences.

Relaxation of the source density ratio could, using readily available gases, accommodate a change in g_o' by a factor of order 10. Using this ratio to our advantage allows the full-scale wind speed being modeled to reduce to $0.95 \times (1000/10)^{1/2} = 9.5$ m/s at $z = \delta$, and to 5.0 m/s at $z = 10$ m. Of course, the range of initial source densities is more restrictive.

(b) *Length scale distortion*: Many of the variables that characterize the near-wall region of a rough-wall turbulent boundary layer (e.g., the mean velocity) scale on distance from the wall rather than the boundary-layer depth. If all the variables scaled on wall distance, then the boundary layer could be used for any length scale ratio between model and full-scale. The use of a smaller length scale ratio, say, 1:100 rather than 1:1000, can extent the range of full-scale situations that may be modeled. The full-scale velocity becomes $0.95 \times \sqrt{100} = 9.5$ m/s at $z = \delta$ or 7.2 m/s at $z = 10$ m. Combination of the length-scale distortion and distortion of the source density ratio gives full-scale velocities of 3.0 m/s at $z = \delta$ and 2.3 m/s at $z = 10$ m. A reduced length-scale distortion restricts the spatial extent that can be modeled in any facility. This distortion does not model the longitudinal and lateral turbulent velocity fluctuations at boundary-layer depth scales. These scales are of less consequence for the dense gas plumes, where plume meandering is not as significant as it is for a neutral plume. Meroney [30] reported good agreement using a 1:85 model in a boundary layer that would have been more correctly used with a far larger scale ratio. If, even with these distortions, the full-scale cannot be modeled, then investigation of modeling at reduced tunnel velocities might be cautiously attempted.

5. Conclusions

1. Extensive experimental data have been obtained for a dense gas plume with significant buoyancy effects but one which was apparently uninfluenced

by molecular properties. The longitudinal decay of the ground-level concentration was similar to that for a passive release, although the plume shapes were quite different. The dense plumes were much wider and flatter than the passive plumes. When $(g_m' \bar{z})^{1/2} > u_*$, the buoyancy-driven lateral velocity produced near-uniform ground-level concentrations across the plume; when $(g_m' \bar{z})^{1/2} < u_*$, ambient turbulence produced a more diffuse edge. Surprisingly, the vertical concentration profiles were nearly exponential, quite distinct from Gaussian or top-hat shapes.

2. The net effect of the dense gas plume encountering a 14° ramp was a slight reduction in the ground-level concentration (about 30% when the ramp was 7.7 ramp heights downstream of the source, and about 40% when the ramp was 2.6 ramp heights downstream). The reductions were similar to those found for neutral plumes; however, the mechanism of concentration reduction was quite different in the two cases. In both cases, increased turbulence contributed to increased dilution of the plumes. In the case of the neutral plume, most of the increased dilution occurred a very short distance up the slope, and this increase was maintained as the plume travelled to the top. In the case of the dense gas plume, the primary mechanism was the increased travel time, which allowed greater lateral spreading of the plume due to its negative buoyancy; little dilution had occurred at the ramp base, but most occurred as the plume was transported to the top of the slope.

3. The main effect of the ramp was to alter the velocity field in which the dense gas plume was developing rather than a direct influence of the ramp slope on the plume.

4. Non-distorted fluid modeling restricts, unsatisfactorily, the range of full-scale situations that may be modeled with confidence. Distorted modeling extends this range to include useful parameter ranges.

Acknowledgements

We are grateful to the staff of the EPA Fluid Modeling Facility for their help through all stages of the work. Particular thanks are due to Mr. Michael Brown and Mr. Malay Jindal for help in collecting the data. Financial support for REB was provided through an appointment as Visiting Associate Professor, Department of Marine, Earth and Atmospheric Sciences, North Carolina State University, under Cooperative Agreement CR 811 973 with EPA, which is acknowledged with thanks.

References

1 F. Pasquill and F.B. Smith, Atmospheric Diffusion, Ellis Horwood, Chichester, England, 3rd edn., 1983, 437 pp.

2 D.B. Turner, Workbook of atmospheric dispersion estimates, Office of Air Programs Pub. No. AP-26, U.S. EPA, Research Triangle Park, NC, 1970.

3 R.E. Britter and R.F. Griffiths, (Eds.), Dense Gas Dispersion, Elsevier, Amsterdam, 1982, 247 pp.

4 R.V. Portelli (Ed.), Heavy Gas, Proc. Heavy Gas (LNG/LPG) Workshop, January 29-30, Toronto, Canada, Concord Scientific Corp., Ontario, Canada, 1985, 294 pp.

5 T. Ellison and J.S. Turner, Turbulent entrainment in stratified flows, J. Fluid Mech., 6 (1959) 432-448.

6 R.E. Britter and P.F. Linden, The motion of the front of a gravity current travelling down and incline, J. Fluid Mech., 99 (1980) 531-543.

7 P. Beghin, E.J. Hopfinger and R.E. Britter, Gravitational convection from instantaneous sources on inclined boundaries, J. Fluid Mech., 107, (1981) 407-422.

8 T.R. Feitz, The measurements of characteristics of a three-dimensional density current, Water Research Laboratory, Report No. 85, University of New South Wales, Kensington, Australia, 1966.

9 D.J. Hall, C.F. Barrett and M.O. Ralph, Experiments on a model of an escape of heavy gas, Report No. CR882(AP), Warren Spring Laboratory, Stevenage, Herts, England, 1974.

10 J.A. Fay and D.A. Ranck, Comparison of experiments on dense gas cloud dispersion, Atmos. Environ., 17 (1983) 239-248.

11 R.G. Picknett, Dispersion of dense gas puffs released in the atmosphere at ground level, Atmos. Environ., 15 (1981) 509-525.

12 R.P. Koopman, R.T. Cederwall, D.L. Ermak, H.C. Goldwire, W.J. Hogan, J.W. McClure, T. McRae, D. Morgan, H. Rodean and J. Shinn, Analysis of Burro Series 40 m^3 LNG spill experiments, J. Hazardous Materials, 6 (1982) 43-83.

13 I.P. Castro and W.H. Snyder, A wind tunnel study of dispersion from sources downwind of three-dimensional hills, Atmos. Environ., 16 (1982) 1869-1887.

14 W.H. Snyder and R.E. Britter, A wind tunnel study of the flow structure and dispersion from sources upwind of three-dimensional hills, Atmos. Environ., 21, (1987) 735-751.

15 R.S. Thompson and W.H. Snyder, Air pollution and terrain aerodynamics: A review of fluid modeling studies at the EPA Fluid Modeling Facility, J. Wind Engineering and Industrial Aerodynamics, 21 (1985) 1-19.

16 R.E. Britter, J.C.R. Hunt, G.L. Marsh and W.H. Snyder, The effects of stable stratification on turbulent diffusion and the decay of grid turbulence, J. Fluid Mech., 127 (1983) 27-44.

17 W.H. Snyder, R.S. Thompson, R.E. Eskridge, R.E. Lawson, Jr., I.P. Castro, J.T. Lee, J.C.R. Hunt and Y. Ogawa, The structure of strongly stratified flow over hills: Dividing-streamline concept, J. Fluid Mech., 152 (1985) 249-288.

18 W.H. Snyder, 1981. Guideline for Fluid Modeling of Atmospheric Diffusion, Report No. EPA-600/8-81-009, U.S. EPA, Research Triangle Park, NC, 1981, 200 pp.

19 W.H. Snyder, The EPA meteorological wind tunnel: Its design, construction, and operating characteristics, Report No. EPA-600/4-79-051, U.S. EPA, Research Triangle Park, NC, 1979, 78 pp.

20 L.J.S. Bradbury and I.P. Castro, A pulsed-wire technique for velocity measurements in highly turbulent flows, J. Fluid Mech., 49 (1971) 657-691.

21 R.E. Lawson, Jr., Standard operating procedures for the EPA Fluid Modeling Facility, FMF Internal Document, U.S. Research Triangle Park, NC, 1984, 132 pp.

22 A.G. Robins, Plume dispersion from ground-level sources in simulated atmospheric boundary layers, Atmos. Environ., 12 (1978) 1033-1044.

23 P.A. Krogstad and R.M. Pettersen, Windtunnel modelling of a release of a heavy gas near a building, Atmos. Environ., 20 (1986) 867-878.

24 R.E. Britter, The ground level extent of a negatively buoyant plume in a turbulent boundary layer, Atmos. Environ., 14 (1980) 779-785.

25 D.L. Ermak, S.T. Chan, D.L. Morgan and L.K. Morris, A comparison of dense gas dispersion model simulations with Burro series LNG spill test results, J. Hazardous Materials, 6 (1982) 129–160.
26 R.E. Britter, Experiments on some effects of obstacles on dense gas dispersion, Safety & Reliability Directorate, Report SRD R407, U.K. Atomic Energy Authority, 1986.
27 J.S. Turner, Buoyancy Effects in Fluids, Cambridge University Press, Cambridge, England, 1973, 368 pp.
28 J.S. Puttock and G.W. Colenbrander, Dense gas dispersion – Experimental research. In: R.V. Portelli (Ed.), Heavy Gas, Proc. Heavy Gas (LNG/LPG) Workshop, Toronto, Canada, January 29–30, Concord Scientific Corp., Ontario, Canada, pp. 32–50.
29 D.E. Neff and R.N. Meroney, The behavior of LNG vapor clouds: Wind-tunnel tests on the modeling of heavy plume dispersion, Final Report No. GRI 80/0145, Gas Research Institute, Chicago, IL, 1982, 120 pp.
30 R.N. Meroney, Guideline for fluid modeling of liquefied natural gas cloud dispersion, Report No. CER84-85RNM-50, Civil Engineering Department, Colorado State University, Ft. Collins, CO, 1985.